American Journal of Biomedical Science and Engineering
2015; 1(1): 1-8
Published online January 30, 2015 (http://www.aascit.org/journal/ajbse)

American Association for Science and Technology

Keywords
Medical Ultrasound,
Apodization,
Windowing Functions,
Linear Array Image Reconstruction,
Phase Array Image Reconstruction

Received: December 28, 2014
Revised: January 16, 2015
Accepted: January 17, 2015

Comparison between windowing apodization functions techniques for medical ultrasound imaging

Mawia A. Hassan

Biomedical Engineering Department, Sudan University of Science & Technology, Khartoum, Sudan

Email address
mawiaahmed@sustech.edu

Citation
Mawia A. Hassan. Comparison between Windowing Apodization Functions Techniques for Medical Ultrasound Imaging. *American Journal of Biomedical Science and Engineering.* Vol. 1, No. 1, 2015, pp. 1-8.

Abstract
Ultrasound imaging is one of the important noninvasive technique that using in medical diagnosis. Unfortunately the far field beam pattern in ultrasound is a sinc function which has a better main-lobe (the resolution of ultrasound imaging) and high side-lobe about -13dB down from the maximum on axis value (the contrast of ultrasound imaging).The result for that is one of a famous artifact in medical ultrasound that the anatomy of the organ outside the main beam to be mapped into the main beam. In this work we used eleven windowing functions to rounded edges of the aperture that taper toward zero at the ends of the aperture to create low side-lobes level and reduce the false echo. Windowing functions used (hamming, hanning, Blackman, Bartlett, Nuttall, Kaiser (β=4,8,12 and 16), Parzen and Bohman) as apodization functions. Images are reconstructed by linear array image reconstruction and raster point technique. To evaluate these eleven windowing functions the SNR is calculated and also the sidelobe and mainlobe in dB are calculated for each window. The results showed that there is trade-off in selecting these function: the main lobe of the beam broadens as the side-lobes lower. However, Nutall, Kaiser (β =12) and Kaiser (β =16) have the best main-lobe, side-lobe and SNR. These windowing functions improve the resolution, contrast of the ultrasound image.

1. Introduction

Ultrasound machines are used in health care to get a picture of what is going on inside the body. The machine use high-frequency sound waves and generate a picture based on how much of the sound is reflected back [1-2]. Ultrasound machines have become very common in hospitals and clinics since these provide very detailed results without the risk that traditional tools and equipment pose. Different approaches and techniques will be done depending on the organ to be studied and the condition of the patient. Ultrasound can also be done in such as short span of time and almost always require no special preparations [3-5].

A commonly used approach to image acquisition in ultrasound system is digital beamforming because the analog delay lines impose significant limitations on beamformer performance and more expensive than digital implementations. Digital beamforming, as applied to the medical ultrasound, is defined as phase alignment and summation [6] of signals that are generated from a common source, by received at different times by a multi-elements ultrasound transducer [7].

The beamforming process needs a high delay resolution to avoid the deteriorating effects of the delay quantization lobes on the image dynamic range and signal to noise ratio (SNR) [8]. If oversampling is used to achieve this timing resolution [9], a huge data volume has to be acquired and process in real time. This is usually avoided by sampling just above the Nyquist rate and interpolating to achieve the required delay resolution [8].

Another beam-forming process, known as 'apodization', can also be employed. In transmission, this involves exciting the elements non-uniformly in order to control the intensity profile across the beam. For example, if the inner elements are excited more than the outer elements, side lobes can be reduced in amplitude and the focal zone can be extended. However, as these benefits are at the expense of a broadening of the main lobe, a compromise is necessary and this is one judgement in which there is no common view among manufacturers. Apodization of the receive beam can be achieved by giving different amplifications to the signals from each element. The receive beam apodization can be changed dynamically to control side lobe characteristics as the receive focus is advanced [10-11].

Unfortunately the far field beam pattern in ultrasound is a sinc function which has a better main lobe (the resolution of ultrasound imaging) and high side-lobe (the contrast of ultrasound imaging).The result for that is one of a famous artifact in medical ultrasound that the anatomy of the organ outside the main beam to be mapped into the main beam. This artifact is known apodization.

The goal of beamforming is to focus ultrasound energy to one location only, but this is not truly achievable with standard delay and sum beamforming. This gives rise to off-axis sidelobes and clutter. These sidelobes or clutter inherent in ultrasound imaging are undesirable side effects since they degrade image quality by lowering CNR and the detectability of small targets.

Improving the contrast of ultrasound has many clinically significant applications. In breast ultrasound, the main purpose is to differentiate solid and cystic masses. Simple anechoic cysts with fill-in caused by multiple scattering, reverberations and clutter can be misclassified as malignant lesions. Levels of fill-in are increased in the presence of aberrations caused by intermittent layers of fat and tissue. Delineation of carcinoma may also be improved with better signal processing methods that improve contrast. Similar problems arise when imaging other soft tissue. For hepatic imaging, visualization of cystic liver lesions and dilated bile ducts can be improved [4]. The visualization of prostate cancer may be improved since prostate cancer is usually hypoechoic [5].

One way to improve CNR is to reduce side-lobe and clutter levels by applying a weighting or shaping function such as a Hanning or Hamming apodization across the transmit and receive apertures. These types of weighting functions are called linear apodization functions since the same weighting is applied to the aperture independent of depth or of imaging line [12-13].

In signal processing, a window function (also known as an apodization function or tapering function) is a mathematical function that is zero-valued outside of some chosen interval. For instance, a function that is constant inside the interval and zero elsewhere is called a rectangular window, which describes the shape of its graphical representation [13].

Any ultrasound echo signal can be thought of as the sum of two signals [13] one signal is the main lobe contribution which is desired and one signal from the side-lobes, grating lobes, and other forms of clutter which reduces image contrast. Side-lobes are unwanted emissions of ultrasound energy directed away from the main pulse. Caused by the radial expansion and contraction of the transducer element during thickness contraction and expansion.Echoes received from side lobes are mapped into the main beam, causing artifacts [14-16].

In this work a comparison between eleven windowing functions to rounded edges of the aperture that taper toward zero at the ends of the aperture to create low side-lobes level and reduce the false echo. The comparison according to the main-lobe, side-lobe and SNR

2. Methodology

2.1. Apodization Windowing Functions

Eleven windowing functions which are: hamming, hanning, blackman, Bartlett, nuttall, Kaiser (β=4, 8, 12 and 16), Parzen and bohman are used (table 1) [17-18].

Table 1. *Apodization Windowing Functions*

Apodization Window	Equation
Hamming	• $w(n) = 0.54 - 0.46\left(2\pi\frac{n}{N}\right)$, $0 \le n \le N$ • The window length L=N+1
Hanning	• $w(n) = 0.5(1 - cos\left(2\pi\frac{n}{N}\right))$, $0 \le n \le N$ • the window length L=N+1
blackman	• $w(n) = 0.42 - 0.5\, cos(2\pi n/(N-1)) + 0.08\, cos\left(^{4\pi n/(N-1)}\right)$, $0 \le n \le M-1$. • Where M=N/2 for N even and (N+1)/2 for N odd.
Nuttall	• $x(n) = a_0 - a_1 \cos\left(2\pi\frac{n}{N-1}\right) + a_2 \cos\left(4\pi\frac{n}{N-1}\right) - a_3 \cos\left(6\pi\frac{n}{N-1}\right)$. • Where n=0,1,2,…N-1.
Flattop	• $x(n) = a_0 - a_1 \cos\left(\frac{2\pi n}{N}\right) + a_2 \cos\left(\frac{4\pi n}{N}\right) - a_3 \cos\left(\frac{6\pi n}{N}\right) + a_4 \cos\left(\frac{8\pi n}{N}\right)$. • Where $0 \le n \le N$ and w(n)=0. • The window length is L=N+1.

Apodization Window	Equation
Kaiser	• To obtain a Kaiser window with sidelobe attenuation of α dB, use the following β. • $\beta = \begin{cases} 0.1102\,(\alpha - 8.7), & \alpha > 50 \\ 0.5842\,(\alpha - 21)^{0.4} + 0.07886(\alpha - 21), & 50 \geq \alpha \geq 21 \\ 0, & \alpha < 21 \end{cases}$
Parzen	• $\begin{cases} 1 - 6(\frac{\lvert n\rvert}{\frac{N}{2}})^2 + 6(\frac{\lvert n\rvert}{\frac{N}{2}})^3\,, & 0 \leq \lvert n\rvert \leq (N-1)/4 \\ 2(1 - \frac{\lvert n\rvert}{\frac{N}{2}})^3\,, & \frac{N-1}{4} < \lvert n\rvert \leq (N-1)/2 \end{cases}$
Bohman	• $w(x) = (1 - \lvert x\rvert)\cos(\pi\lvert x\rvert) + \frac{1}{\pi}\sin(\pi\lvert x\rvert)$. • $where\ -1 \leq x \leq 1$.

2.2. Digital Beamforming Steps

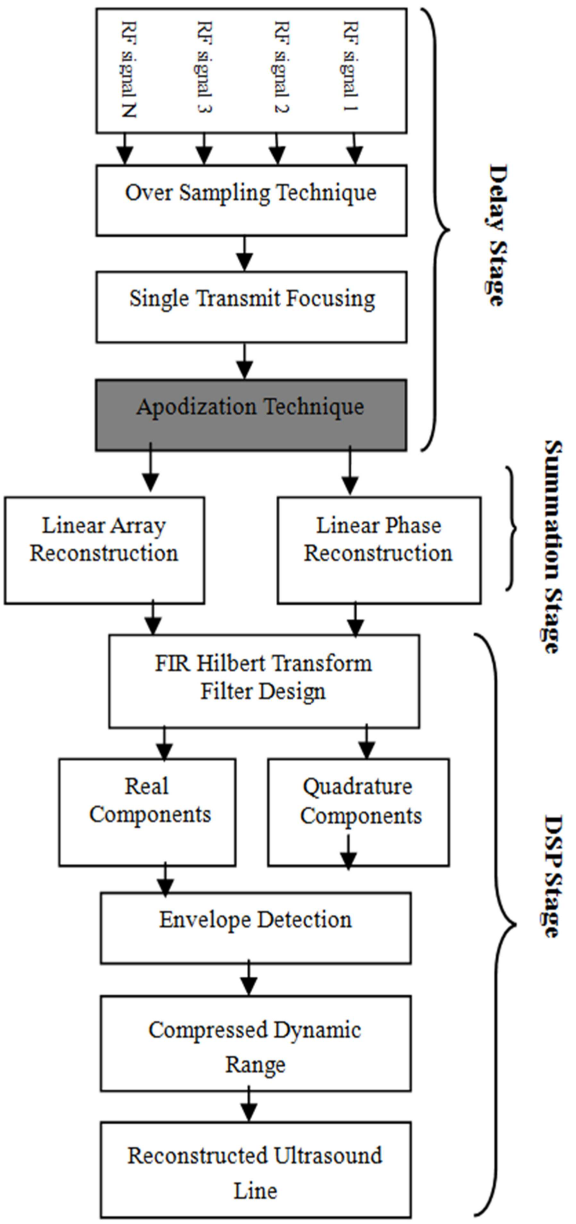

Fig. 1. Digital Beamforming Steps [19]

Digital beamforming, as applied to the medical ultrasound, is defined as phase alignment and summation of signals that are generated from a common source, by received at different times by a multi-elements ultrasound transducer. After delay and sum the envelope of the signals is detected. The envelope then compressed logarithmically to reduce the dynamic range because; the maximum dynamic range of the human eye is in the order of 30 dB. The actual dynamic range of the received signal depends on the ADC bits, the time gain compensation (TGC) amplifier used in the front end, and the depth of penetration. The signal is compressed to fit the dynamic range used for display (usually 7 or 8 bits). It is typical to use a log compressor to achieve the desired dynamic range for display (Fig 1)[19].

2.3. Linear Array Image Reconstruction

Electronic focusing was applied on receive for each aperture (AP). Received at the AP elements are delayed by focusing delays and summed to form scan line in the image. After that one elements shift is applied to the AP and the process was repeated till the end of the array elements at the outer side processing all image scan lines (Fig.2 where aperture equal 32 elements). The number of lines equal to the total number of elements minus the number of the aperture elements plus one [19].

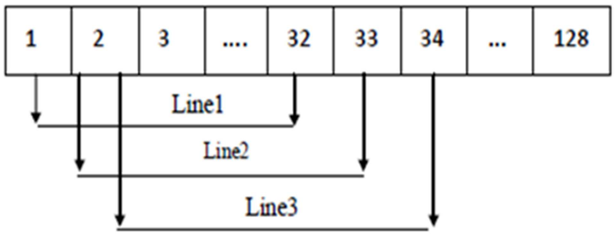

Fig. 2. Linear physical image reconstruction

2.4. Linear Phase Array Reconstruction

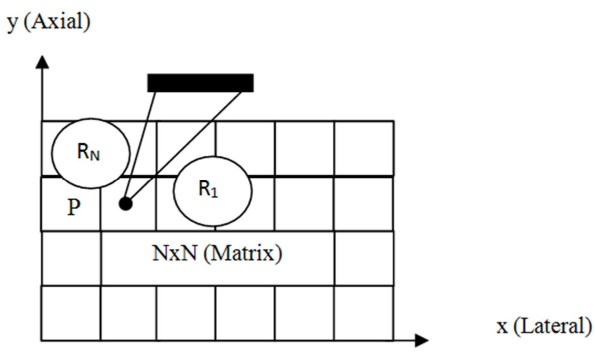

Fig. 3. The raster point technique

In contrast the linear array, phase array transducer required that the beamformer steered the beam with an unswitched set of array elements. In this process, the time shifts follow a linear pattern across of array from one side to another side. In receive mode, the shifted signals are summed together after phase shift and some signal conditioning to produce a single output. This reconstruction technique divides the field of view (FOV) into different point targets (raster points), P(i,j) [19].

Each point represented as an image pixel, which is separated laterally and axially by small distances. Each target is considered as a point source that transmits signals to the aperture elements as in fig.3. The beamforming timing is then calculated for each point based on the distance R between the point and the receiving element, and the velocity of ultrasonic beam in the media. Then the samples corresponding to the focal point are synchronized and added to complete the beamforming as the following [19]:

$$P_D(i,j) = \sum_{n=1}^{N} X_n\left(K_{ij}\right), \qquad (1)$$

where P_D (i,j) is the signal value at the point whose its coordinates are (i,j), and $X_n(K_{ij})$ is the sample corresponding to the target point in the signal X_n received by the element number n. The sample number K_{ij} which is equivalent to the time delay is calculated using the equation below [19]:

$$K_{ij} = \frac{R_n(i,j)}{T * c}. \qquad (2)$$

Here R_n (i, j) is the distance from the center of the element to the point target, c is the acoustic velocity via the media, and T is the sampling period of the signal data.

3. Results and Discussions

3.1. The Real Data

We used correct data obtained from the Biomedical Ultrasound Laboratory, University of Michigan [20]; the phantom data set that was used to generate the results here is under "Acusonl7". The parameters for this data set are as follows: the number of channels was 128 channels, and the A/D sampling rate was 13.8889 MSPS. Linear shape transducer was used to acquire the data with center frequency of 3.5 MHz, and element spacing of 0.22mm. Each ultrasonic A-scan was saved in a record consisted of 2048 RF samples per line each represented 4 byte for the real data, and the signal averages was 8. The speed of the ultrasound was 1480 m/sec. The data were acquired for phantom within 6 pins at different positions.

3.2. The Effect of Apodization Filters

Fig. 4 shows Comparison between apodized and non apodized aperture using different windowing functions. Because the aperture is rectangular unfortunately, the far field beam pattern is a sinc function with near in-side lobes only -13 dB down from the maximum on axis value.

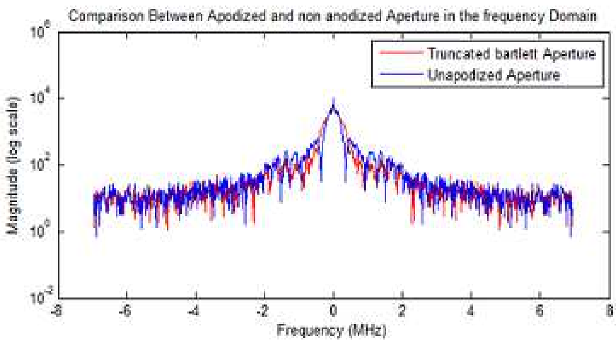

(a)

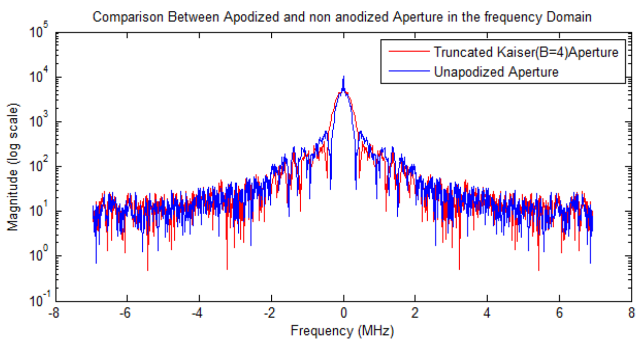

(b)

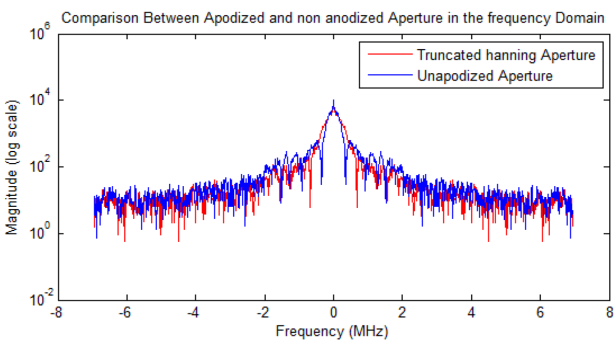

(c)

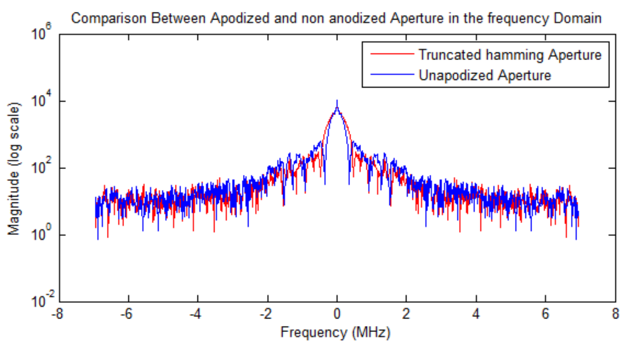

(d)

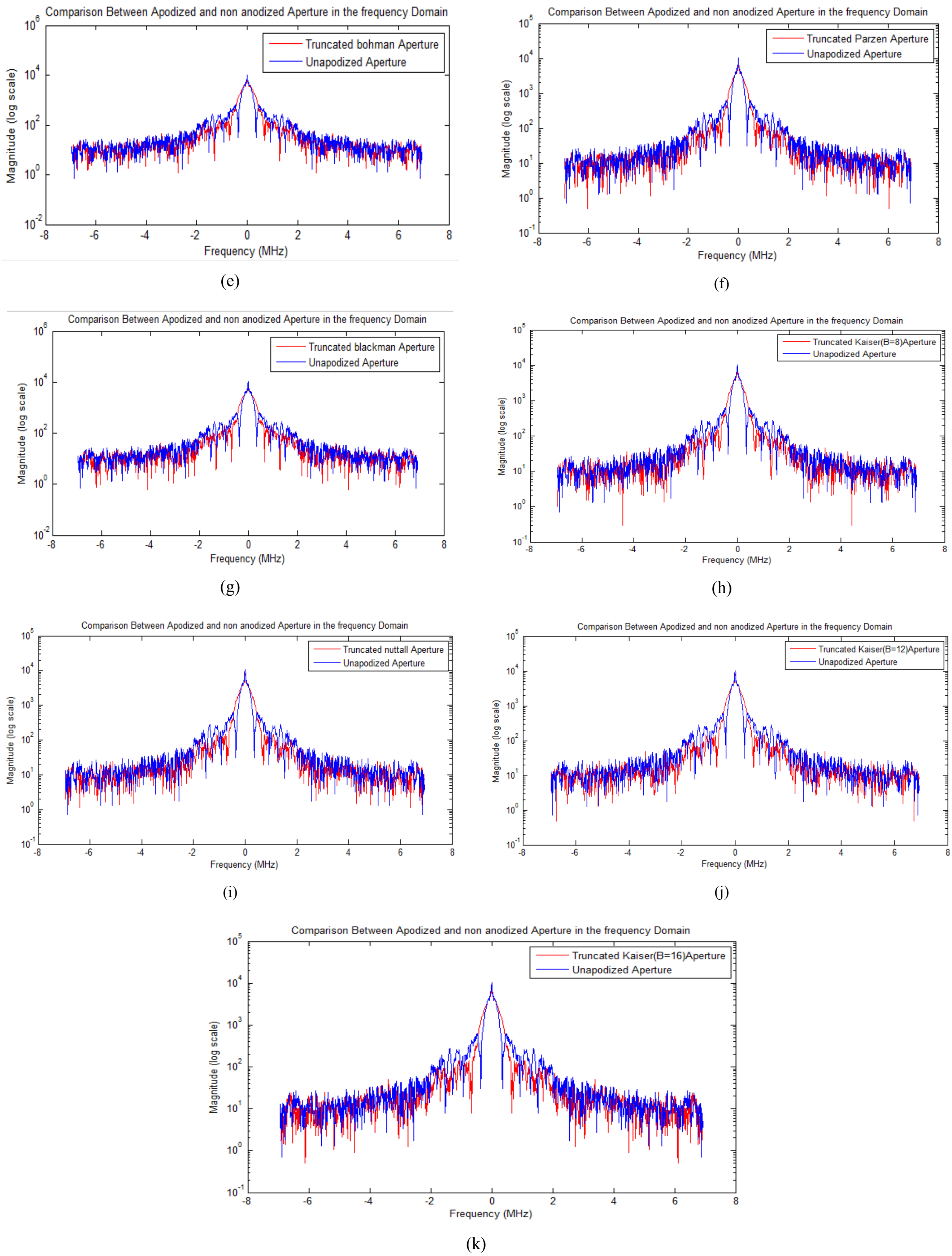

Fig. 4. *Comparison between apodized and non apodized aperture using different windowing. (a) Bartlett, (b) Kaiser β =4, (c) Hanning, (d) Hamming, (e) Bohman, (f)Parzen, (g) Blackman, (h) Kaiser β =8, (i)Nutall, (j)Kaiser β =12 and (k)Kaiser β =16*

Fig. 5 show pin three in the phantom as a sub-image which are reconstructed by phase array image reconstruction (Fig.3) (raster point technique). Fig.6 show linear array image reconstruction (Fig.2). The comparison between images reconstructed without apodization (Fig. 5a and Fig.6a) to images reconstructed with apodization. As can be shown there is trade-off in selecting these functions: the main lobe of the beam broadens as the side lobes lower compared to figure 5a and Fig.6a for rectangular aperture. In Fig. 5 and Fig.6 the Kaiser with β =16 gave the best side lobe and the best field of view (figure 5-l) and the image without apodization (rectangular window) gave the worst side lobe and field of view.

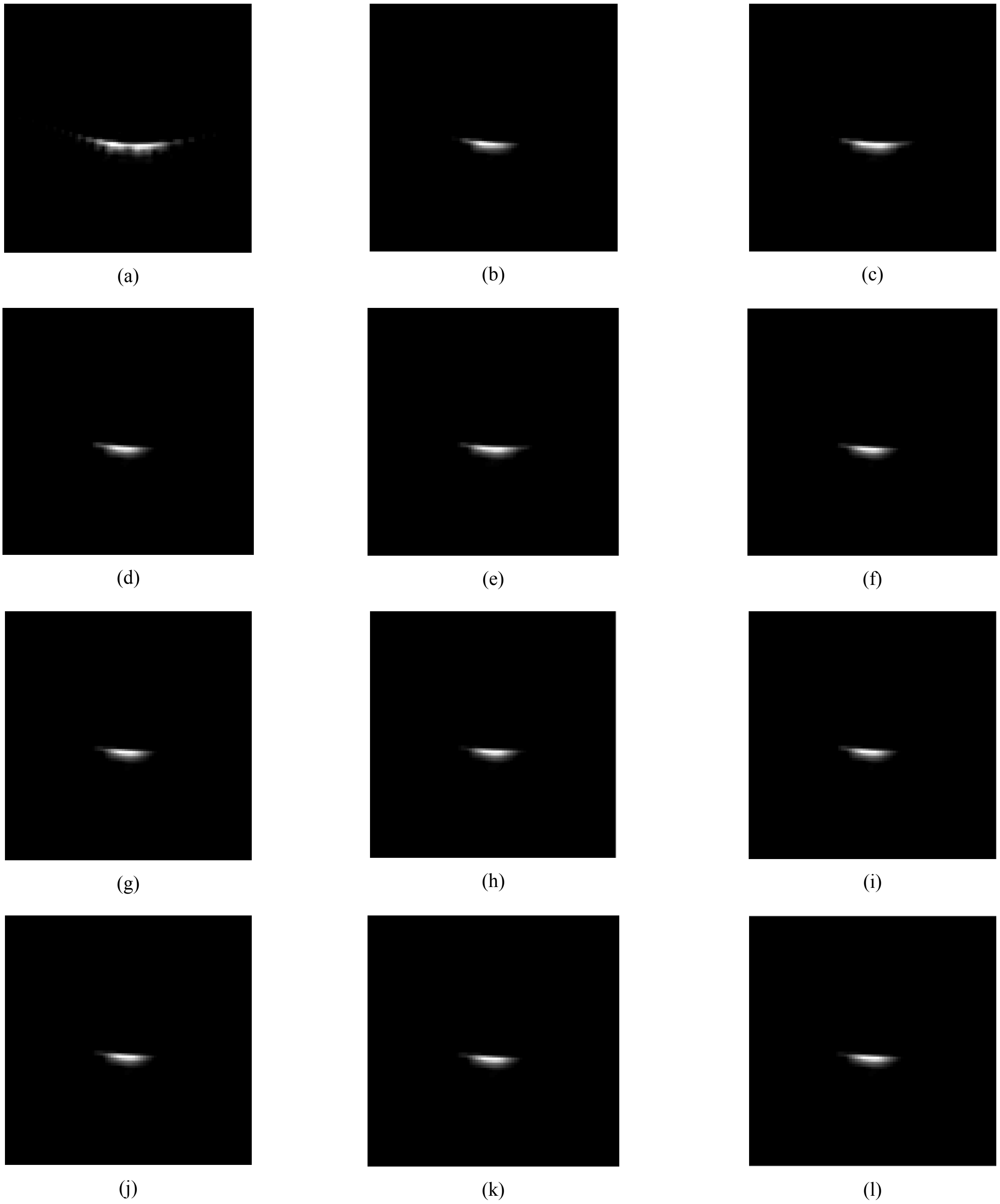

Fig. 5. *Phase array image reconstruction with and without apodization (a) without-apodization (b) Bartlett, (c) Kaiser β =4, (d) Hanning, (e) Hamming, (f) Bohman, (g) Parzen, (h) Blackman, (i) Kaiser β =8, (g) Nutall, (k) Kaiser β =12 and (l) Kaiser β =16.*

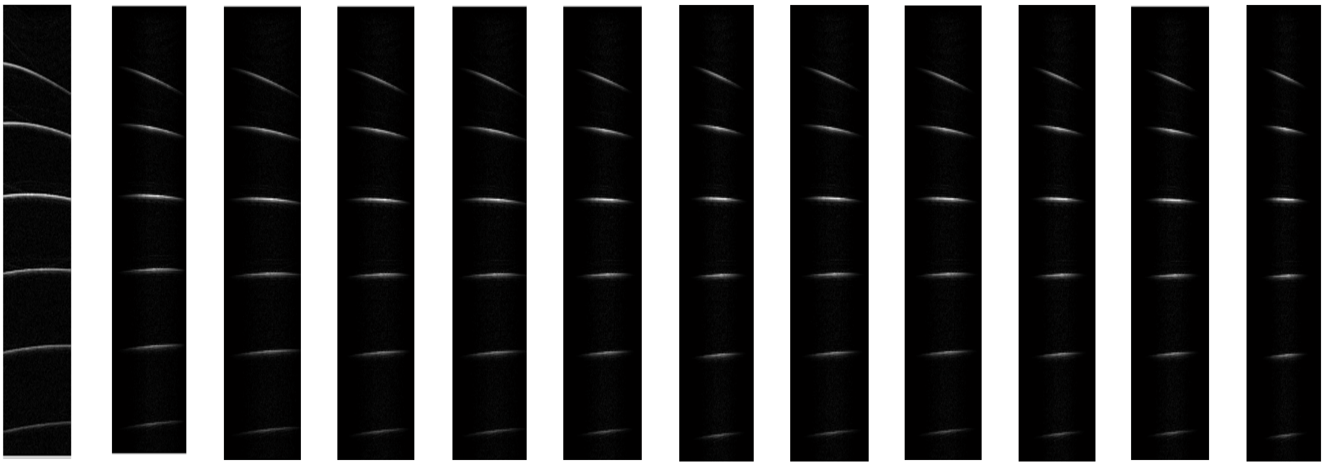

(a) (b) (c) (d) (e) (f) (g) (h) (i) (j) (k) (l)

Fig. 6. *Linear array image reconstruction with and without apodization (a) without apodization (b) Bartlett, (c) Kaiser β =4, (d) Hanning, (e) Hamming, (f) Bohman, (g) Parzen, (h) Blackman, (i) Kaiser β =8, (j) Nutall, (k) Kaiser β =12 and (l)Kaiser β =16.*

Table 2. *Comparesion between the windowing function*

Window	Main-lobe -3 db	Side-lobe db	SNR(relative)
Rectangular	0.0136	-13dB	32.6679
Hamming	0.0195	-42.6	37.6472
Hanning	0.0215	-31.6	40.8508
Black man	0.0254	-58.1	38.4245
Bartlett	0.0195	-26.5	39.8609
Parzen	0.0273	-53.1	41.6557
Nutall	0.0293	-69.8	41.7056
Bohman	0.0254	-46	41.5308
Kaiser β =4	0.0176	-30.3	37.0414
Kaiser β =8	0.0234	-58.4	41.2967
Kaiser β =12	0.0293	-90.2	41.7328
Kaiser β =16	0.0332	-122.2	41.7867

Table 3. *The order of the windowing functions*

Side-lobe	SNR	Main-lobe
a) Without Apodization	Without Apodization	Without Apodization
b) Bartlett	Kaiser β =4	Kaiser β =4
c) Kaiser β =4	Hamming	Hamming
d) Hanning	Black man	Bartlett
e) Hamming	Bartlett	Hanning
f) Bohman	Hanning	Kaiser β =8
g) Parzen	Kaiser β =8	Black man
h) Blackman	Bohman	Bohman
i) Kaiser β =8	Parzen	Parzen
j) Nutall	Nutall	Nutall
k) Kaiser β =12	Kaiser β =12	Kaiser β =12
l) Kaiser β =16	Kaiser β =16	Kaiser β =16

The comparison between these function can be shown in table 2. The comparison is according the main lobe (the image resolution), the side lobe (the image contrast) and the relative SNR. Table 3 shows the order of the windows according to the comparison in table 1. As can be shown Nutall, Kaiser (β =12) and Kaiser (β =16) have the best main-lobe, side-lobe and SNR.

4. Conclusion

In this study a comparison between some windowing functions to use as apodization technique for medical ultrasound imaging. From the results after applied the windowing functions Nutall, Kaiser (β =12) and Kaiser (β =16) have the best main-lobe, side-lobe and SNR. These windowing functions improve the resolution, contrast of the ultrasound image.

References

[1] Desser TS, Jedrzejewicz T, Bradley C (2000) Native tissue harmonic imaging: basic principles and clinical applications. *Ultrasound Quarterly,* 16, 40 –8.

[2] Dickinson RJ (1986). Refl ection and scattering. In CR Hill, ed., *Physical Principles of Medical Ultrasonics* .

[3] Chichester: Ellis Horwood. Duck FA (1990). *Physical Properties Of Tissue – A Comprehensive Reference Book.* London: Academic Press.

[4] Duck FA (2002). Nonlinear acoustics in diagnostic ultrasound. *Ultrasound in Medicine and Biology,* 28, 1 –18.

[5] Humphrey VF (2000). Nonlinear propagation in ultrasonic fields: measurements, modeling and harmonic imaging. *Ultrasonics,* 38, 267 –72.

[6] J. A Zagzebski, Essentials of ultrasound physics, St Louis, Mo: Mosby, (1996).

[7] R. Reeder, C. Petersen, The AD9271-A Revolutionary Solution for Portable Ultrasound, Analog Dialogue, Analog Devices. (2007).

[8] C. Fritsch, M. Parrilla, T. Sanchez, O. Martinez, "Beamforming with a reduced sampling rate," Ultrasonics, vol. 40, pp. 599–604, 2002.

[9] B. D. Steinberg, "Digital beamforming in ultrasound," IEEE Transactions on Ultrasonics, Ferroelectrics and Frequency Control, vol. 39, pp. 716–721, 1992.

[10] Th omenius KE (1996). Evolution of ultrasound beamformers. *IEEE Ultrasonic Symposium Proceedings,* 1615 –22.

[11] Shattuck DP, Weinshenker MD, Smith SW, von Ramm OT (1984). Explososcan: a parallel processing technique for high speed ultrasound imaging with linear phased arrays. *Journal of the Acoustical Society of America,* 75, 1273 –82.

[12] The Gale Encyclopedia of Medicine, 2nd Edition, Vol. 1 A-B. p. 4, Cobbold, Richard S. C. (2007). Foundations of Biomedical Ultrasound. Oxford University Press. pp. 422–423. ISBN 978-0-19-516831-0.

[13] Chi Hyung Seo,"Improved contrast in ultrasound imaging using dual apodization with cross-correlation", presented to the faculty of the viterbi school of engineering university of southern California, December 2008.

[14] Eric W. Weisstein (2003). CRC Concise Encyclopedia of Mathematics. CRC Press. ISBN 1-58488-347-2.

[15] Hoskins PR, Th rush A, Martin K, Whittingham TA. (2003). *Diagnostic ultrasound physics and equipment.* London: Greenwich Medical Media.

[16] M. Ali, D. Magee and U. Dasgupta, "Signal Processing Overview of Ultrasound Systems for Medical Imaging," SPRAB12, Texas Instruments, Texas, November 2008.

[17] J. O. Smith, Mathematics of the Discrete Fourier Transform (DFT), Center for Computer Research in Music and Acoustics (CCRMA), Department of Music, Stanford University, Stanford, California, 2002.

[18] A. V. Oppenheim and R. W. Schafer, Discrete-Time Signal Processing. NJ: Prentice-Hall, Englewood Cliffs, 1989.

[19] Mawia A. Hassan and Yasser M. Kadah, "Digital Signal Processing Methodologies for Conventional Digital Medical Ultrasound Imaging System," Proc. American Journal of Biomedical Engineering, vol. 3(1), pp. 14-30, USA, 2013

[20] M. O'Donnell and S.W. Flax, "Phase-aberration correction using signals from point reflectors and diffuse scatterers: measurements," IEEE Trans. Ultrason., Ferroelect., and Freq. Contr. 35, no. 6, pp. 768-774, 1988